PAPER • OPEN ACCESS

Elliptical generalized Maxwell fish-eye lens using conformal mapping

To cite this article: Hossein Eskandari *et al* 2019 *New J. Phys.* **21** 063010

New Journal of Physics
The open access journal at the forefront of physics

Deutsche Physikalische Gesellschaft DPG
IOP Institute of Physics

Published in partnership with: Deutsche Physikalische Gesellschaft and the Institute of Physics

OPEN ACCESS

RECEIVED
22 December 2018

REVISED
2 May 2019

ACCEPTED FOR PUBLICATION
24 May 2019

PUBLISHED
11 June 2019

PAPER

Elliptical generalized Maxwell fish-eye lens using conformal mapping

Hossein Eskandari[1], **Mohammad Saeed Majedi**[1], **Amir Reza Attari**[1] and **Oscar Quevedo-Teruel**[2]

[1] Department of Electrical Engineering, Ferdowsi University of Mashhad, Mashhad, Iran
[2] Department of Electromagnetic Engineering, KTH Royal Institute of Technology, Stockholm, Sweden

E-mail: Hossein.skandari@gmail.com

Keywords: transformation optics, conformal transformation, Maxwell fish-eye

Abstract

A circular graded index lens is conformally transformed to an elliptical shape using a closed-form transformation. The proposed transformation is then employed to compress a Maxwell fish-eye and its generalized version. Since the transformation is conformal, the electromagnetic properties of the device are perfectly preserved after the transformation with fully isotropic and dielectric-only materials. Ray-tracing and full-wave simulations are carried out for several cases to verify the functionality of the optically transformed lenses in geometrical optics and wave optics regimes.

1. Introduction

Graded index (GRIN) media are commonly employed for the design of electromagnetic devices from optics to the microwave regime [1–3]. GRIN devices, when implemented with dielectric materials, offer a wide-band functionality [4, 5]. There are several common methods to fabricate an all-dielectric non-homogeneous GRIN medium. Some of these methods are drilling sub-wavelength holes in a sufficiently high refractive index substrate [4, 6, 7], suspension polymerization technique [8, 9], dielectric layered shell deposition [10–12], ion-exchange method on optical glasses [13], parallel waveguide plate height modification for mode index alteration [14–16], modification of the guiding silicon substrate height [17, 18], graded photonic crystals [19–22] and electron-beam lithography (EBL) [18, 23–26]. Alternatively, mushroom structures [27], bed of nails [28, 29], holey structures [30] and non-uniform metallic patches over a dielectric layer [31] are tested and verified in the microwave regime to provide variable refractive index over a spatial region.

Rotationally symmetric GRIN lenses are known for their abberation less performance. Some notable examples are the Maxwell fish-eye (MFE) [32], generalized MFE (GMFE) [33], Eaton [34, 35], invisible [36, 37] and Luneburg lenses [38].

The MFE was proposed by Maxwell as a spherically symmetric refractive index profile that can focus the light rays passing through a point in space to a corresponding image point stigmatically [32]. This device is considered as an absolute optical instrument since the lens is abberation free and it produces an optimal response within ray optics [35]. The refractive index of this optical lens is:

$$n(r) = \frac{2n_0}{1 + (r/a)^2}, \tag{1}$$

where r is the distance from the lens center and n_0 is the background refractive index. Also, parameter a scales the refractive index and can be taken as a virtual radius of the lens. It is important to remark that the light rays in this device follow circular paths. The MFE focuses the rays from a source point at position $\mathbf{r}$ to the point $-\mathbf{r}a^2/\mathrm{r}^2$.

It was later demonstrated that the perfect imaging properties of this lens are due to the fact that the device performs a stereographic projection from the surface of a sphere to a plane where circles on a sphere are mapped to circles on the plane [38]. Since rays emitted from a point on the surface of a sphere get focused on a conjugate point following the orthodromes, same thing happens for the corresponding circles on the projected plane

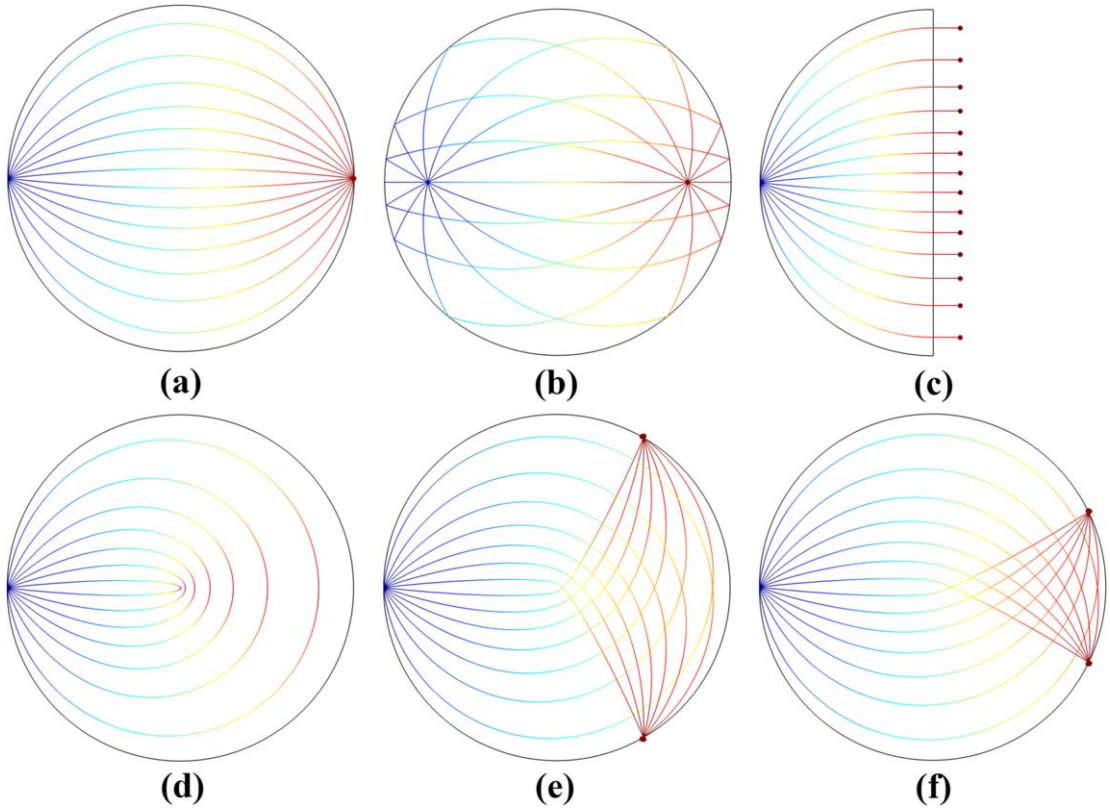

Figure 1. Schematic of ray trajectories for several lenses. (a) MFE. (b) Mirrored MFE with a source point at $-3a/4$. (c) HMFE. (d) GMFE with $m = 1/2$ (monopole lens). (e) GMFE with $m = 6/8$. (f) GMFE with $m = 7/8$.

[38, 39]. To make the MFE more suitable for practical applications, the use of a mirror in contour of the lens was proposed. Perfect imaging properties of an unbounded MFE are also obtained in a bounded mirrored MFE [40–42]. In figures 1(a) and (b) the trajectory of the rays inside a MFE and a mirrored MFE, for excitation points on the lens contour and inside the lens, is illustrated. There is an ongoing debate among scientists if the imagining properties of this lens can be extended from ray optics to wave optics, leading to sub-wavelength imaging. There are numerous papers that either support the idea of sub-wavelength imaging by MFE [43–48] or disagree with it [46, 49–54]. The focusing properties of the two-dimensional (2D) MFE lens were experimentally confirmed with prototypes where Ion-exchange [13], EBL [24, 26] and 3D printing for parallel plates waveguide height modification [14] were employed. Furthermore, since the MFE provides a point-to-point focus, it has been demonstrated to be efficient for photonic waveguide couplers. A metamaterial-based version of the MFE has been recently fabricated and tested as a waveguide crossing [55]. Similarly, a MFE waveguide intersection based on photonic crystals has demonstrated to provide promising coupling efficiencies in simulations for photonic applications [21, 22].

The half MFE is simply a MFE that is cut in half. This lens has been used to produce highly directive antennas [12, 56–61]. The ray trajectories for this lens are depicted in figure 1(c). Although this solution was intended for directive antennas, it has two limitations. The first one is that it is only appropriate for the central excitation point, and its properties degrade for extreme angles. Additionally, the contour at the opposite direction of the feeding is not matched to vacuum leading to reflections that reduce the radiation efficiency. These two limitations were overcome by Luneburg with his proposed lens while sacrificing the compactness [38].

The generalized Maxwell fish-eye (GMFE), on the other hand, is a more general concept than the lens originally proposed by Maxwell. The refractive index profile for this lens is [33]:

$$n(r) = \frac{2}{(r/a)^{1-m} + (r/a)^{1+m}}, \tag{2}$$

where for a fractional representation of m as $m = \nu_1/\nu_2$, the ray emitting from a source at position $\mathbf{r}$ revolves $\nu_2/2$ times around the center before it gets focused: (1) at the point $-\mathbf{r}a^2/r^2$ if ν_1 and ν_2 are odd, (2) at point $\mathbf{r}a^2/r^2$ if ν_1 is odd and ν_2 even, and (3) at the point $-\mathbf{r}$ if ν_1 is even and ν_2 odd [33]. For instance, for $m = 1$, we have the original MFE lens. The monopole lens is achieved when $m = 1/2$. This lens focuses a ray emitting from

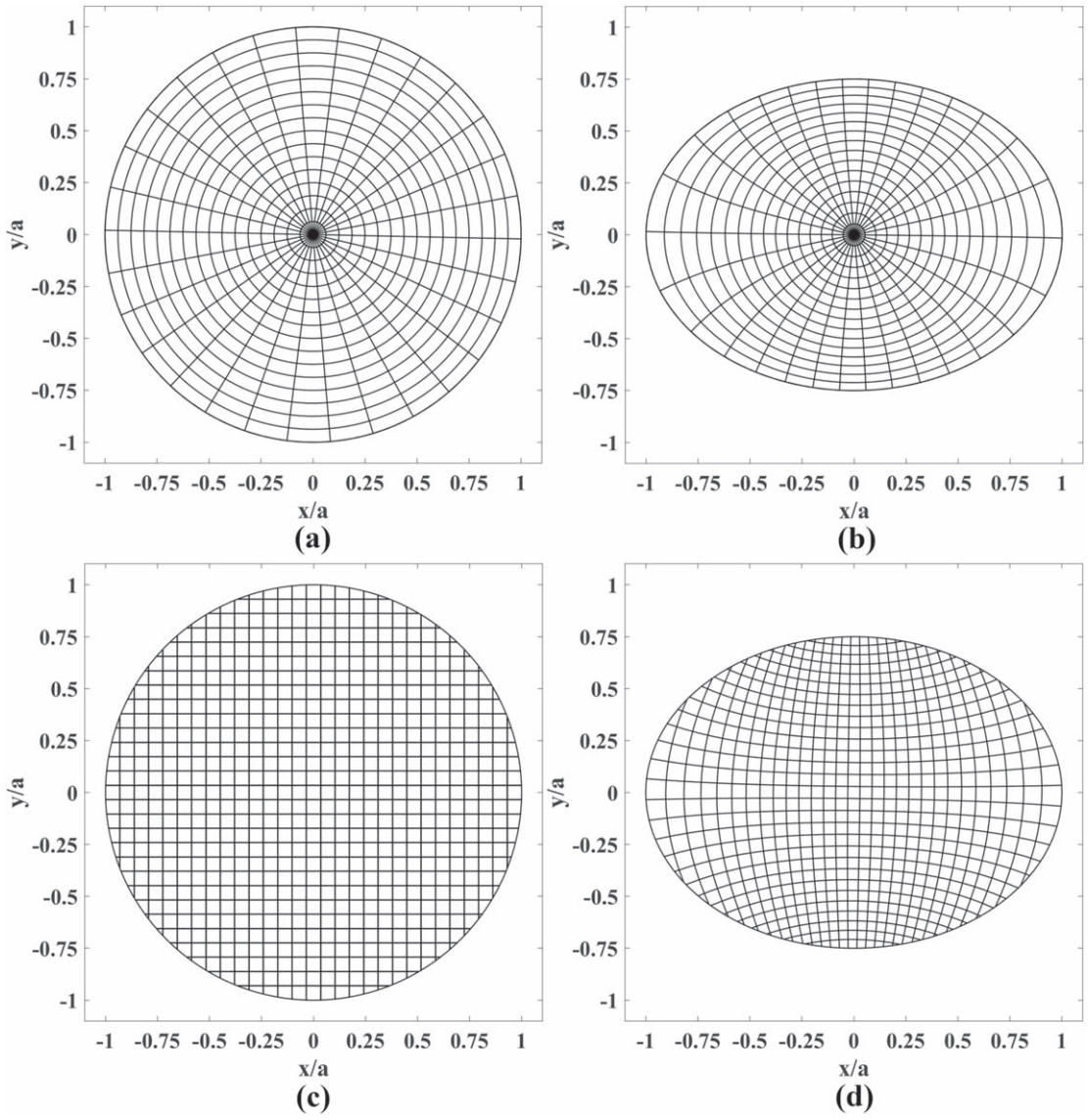

Figure 2. Conformal mapping of grids from a circle to an ellipse for the compression ratio of 3/4. (a) Cylindrical grids inside the circle. (b) Transformed cylindrical grids inside the ellipse. (c) Cartesian grids inside the circle. (d) Transformed Cartesian grids inside the ellipse.

a point on the lens contour back to its source after a single revolution around the center, as depicted in figure 1(d). The GMFE lens can also split the rays emitting from a point source into two points of the lens contour with a variable distance. Two examples of power splitting with GMFE are shown in figures 1(e) and (f). An example of the GMFE has been recently fabricated using a polymer/ceramic composite for beam splitting [62].

Although the optical properties of the GMFE present a great potential for various functionalities, some researchers have shown interest to investigate the possibilities of changing the geometry of this lens to make it more suitable for practical applications or, in some cases, less bulky. Maintaining the functionality of the lens while reshaping it, is an active research field. In this particular subject, transformation optics (TO) proves to be a very powerful tool.

TO permits a geometry modification of an optical device while maintaining its electromagnetic characteristics. Basically, TO relates the electromagnetic fields and material parameters of two spaces namely, virtual and physical spaces. The virtual space is the trivial space in which the behaviour of the device is known e.g. a circular GMFE or the vacuum. By applying a transformation to the virtual space, one can reshape it to a desired geometry called physical space. The geometry change is embodied into the material parameters in the physical space following a specific recipe. The formulation to calculate the physical space medium is described in appendix A. An important part of the TO literature, rather that reshaping geometries for the common lenses, has

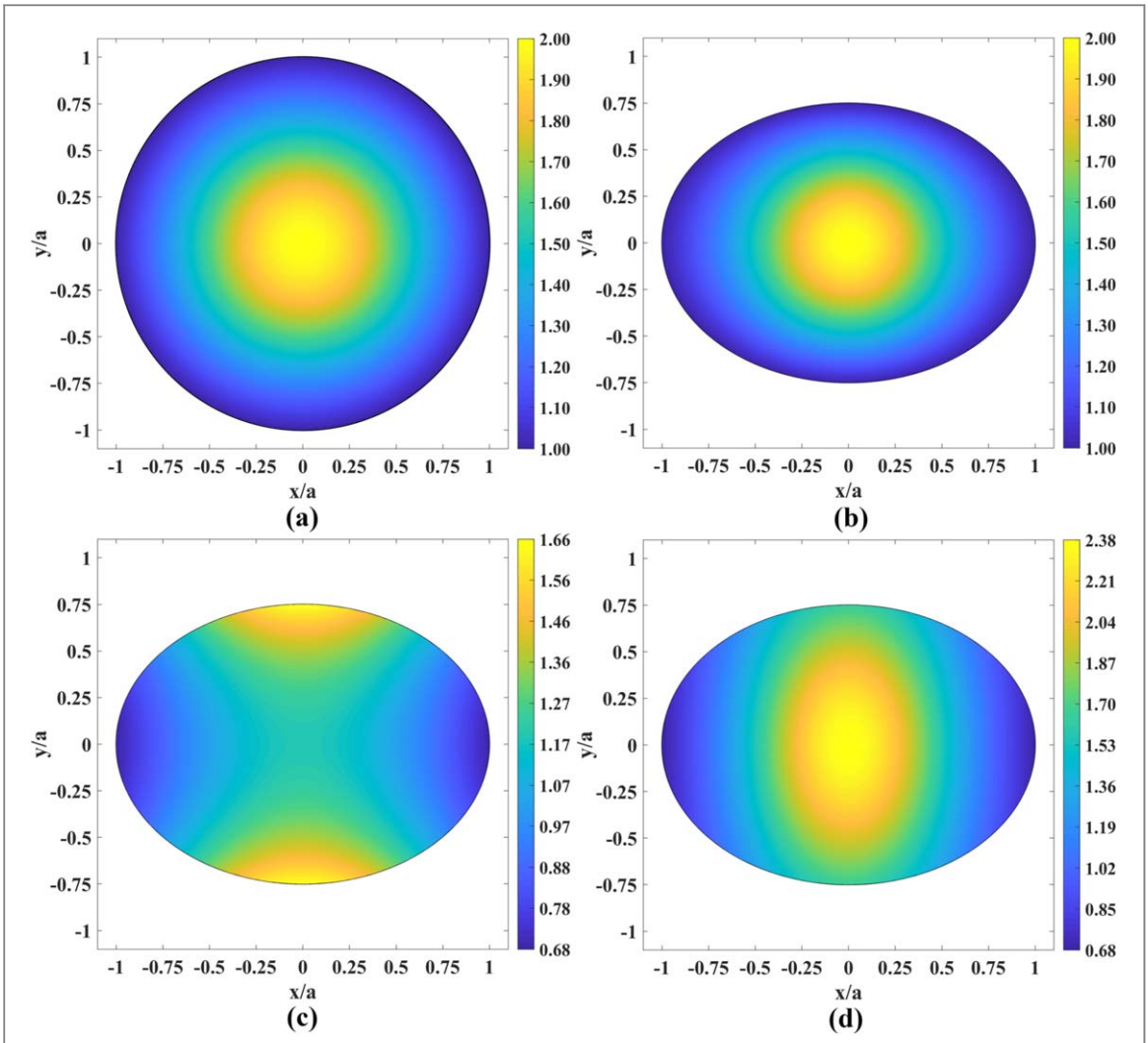

Figure 3. Index calculation steps for the transformation of a circular to elliptical MFE lens with the compression ratio of 3/4. (a) Circular MFE index profile. (b) Point to point index map form the circle to the ellipse $n(u, v)$. (c) Pure map index $|f'(z)|$. (d) Final elliptical index profile $n(x, y)$.

been focused on designing of new devices with exceptional functionalities. The most notable one is the invisibility cloak [6, 63–72]. Furthermore, numerous devices have been designed using TO including polarization splitters [73–78], phase transformers [79–81], flat lenses [4, 82–91], field rotators [92, 93], field concentrators [94–96], waveguide bends [97–99] and waveguide couplers [100–107].

Despite the promising freedom that TO provides for the design of new devices, the general formulation of TO usually leads to extreme materials that are anisotropic, non-homogeneous and may require magnetic materials. Also, the values of the material permeability and permittivity may be extreme, i.e. infinite, near zero or negative. To facilitate the practical realization, special types of transformations are used, namely, conformal and quasi-conformal [64, 71, 108–110]. These two types of transformation mitigate the requirement of anisotropy and lead to a possible implementation with only dielectric materials for one polarization. This is because in the conformal or quasi-conformal transformation, the mapping formula satisfies fully, or partially, the Cauchy–Riemann conditions. The conformal method is, in most cases, based on a closed-form representation of the mapping, while the quasi-conformal approach includes numerical calculation. Conformal and quasi-conformal mappings have been employed for various purposes including attaining high directivity antennas in the microwave regime [19, 87, 90, 111–115], reflectors with flat boundaries [116–118] and all-dielectric bends [98, 108, 111, 112].

For the case of the MFE, quasi-conformal transformations have been employed to flatten the image and feeding planes [119]. One example of this concept was fabricated with non-resonant metamaterial structures to produce a broadband relay lens [120]. A similar approach was also conducted to produce a MFE suitable for integrated photonics as a flat cross coupler [114]. The conformal Schwarz–Christoffel mapping was also

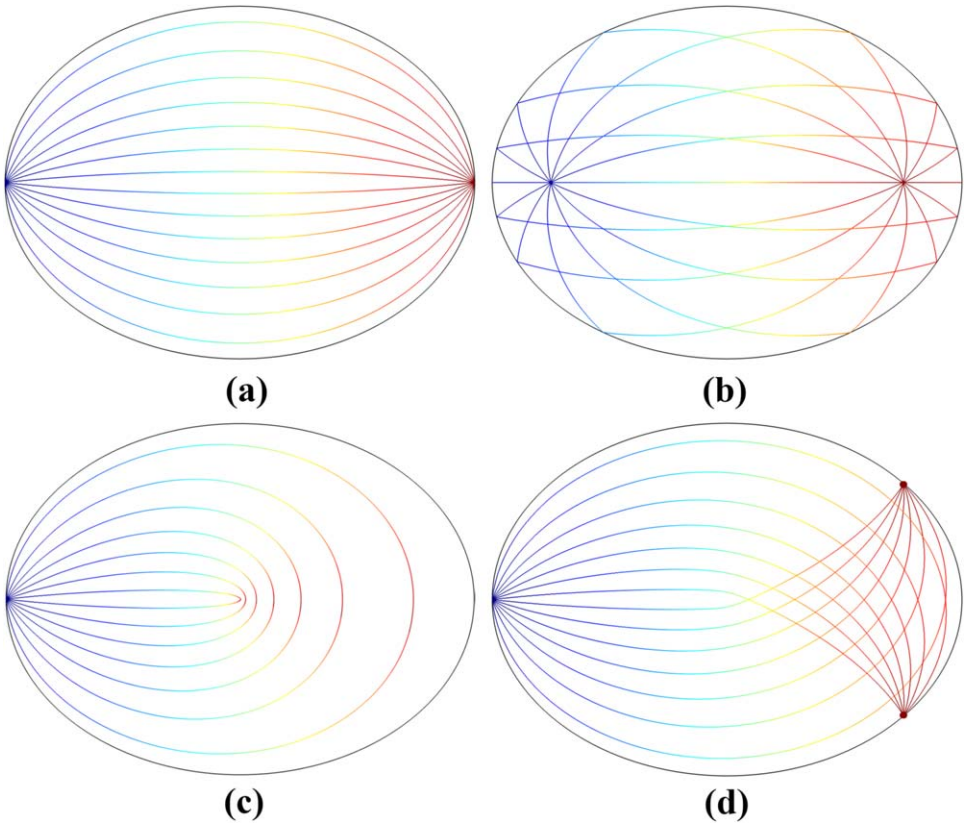

Figure 4. Ray-tracing simulations for an elliptical MFE lens with the compression ratio of 3/4. (a) Elliptical MFE. (b) Mirrored MFE excited at point $(-3/4m, 0)$. (c) GMFE with $m = 1/2$ (monopole lens). (d) GMFE with $m = 7/8$.

employed to create a MFE with relatively big rectangular shape and a prototype of the lens was implemented with fractal metamaterials [121]. Recently, a semi-analytical conformal method was proposed to produce a universal waveguide crossing with flat output ports that was fabricated using EBL [122]. The circular MFE was transformed conformally to a square via a closed-from formula, demonstrating its performance in both ray and wave optics [123]. Also, it is known that the MFE is connected to a Mikaelian lens through an exponential conformal map [124, 125]. Hence, the Mikaelian lens can be considered as a conformally mapped version of the MFE. The self-focusing and Talbot effects of such lens have been experimentally investigated, demonstrating that Mikaelian lenses can be engineered to transmit digital data without diffraction [126].

Compressing a lens size via TO is still an active research field. For example, TO was used to compress the space in one direction [85]. However, anisotropy and magnetic materials are needed in this case. This drawback is shared in other works in which a conversion from a circular shape to an elliptical one was aimed [127, 128]. However, anisotropy will not exist if a conformal map is used. Additionally, the final device can be implemented with only dielectric materials. In this paper, we propose the use of a unique closed-form formula for the conformal transformation of an ellipse to a circle and vice versa. The formula is then used to transform circular MFE and GMFE lenses to an ellipse with a given compression ratio. As a consequence of the conformal mapping, the resulting compressed lens can be implemented with only dielectrics. The performance of the device is evaluated by a number of examples using ray-tracing and full-wave simulations.

2. Elliptic MFE and GMFE lenses

Details on the calculation of the conformal mapping between an ellipse and a circle are thoroughly explained in the appendices B and C. The mapping from an ellipse to a circle is expressed in equation (C.6) whereas the inverse mapping is expressed in equation (C.8). Figure 2 illustrates how cylindrical and Cartesian grids inside a circle are mapped to an ellipse. The compression ratio here is 3/4 ($a = 1$ and $b = 3/4$). The coordinate lines are mapped to the ellipse while preserving their relative perpendicular angles. This is due to the angle-preserving

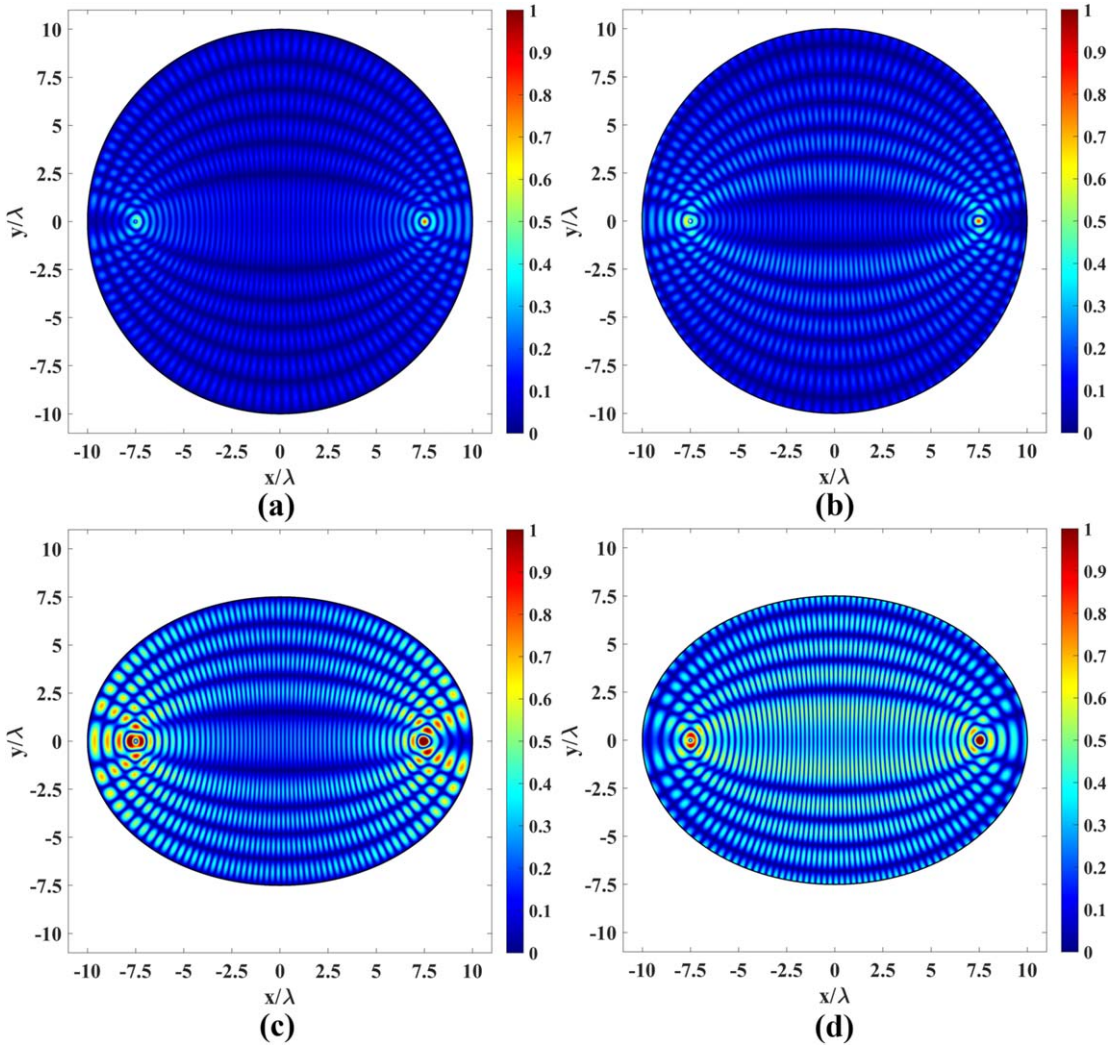

Figure 5. Normalized magnitude of the fields for the mirrored circular and elliptical MFE lenses for TE and TM polarizations. The excitation is applied at $(-3/4m, 0)$. (a) Magnitude of E_z and (b) magnitude of H_z for the circular MFE. (c) Magnitude of E_z and (d) magnitude of H_z for the elliptical MFE.

feature of conformal mapping that isotropically maps the coordinate lines from one shape to another and produces no anisotropy in the physical space.

The refractive index for a circular MFE and optically transformed elliptical MFE are shown in figure 3. The final map, $n(x, y)$ is calculated through equations (A.8) and (C.7), by using the point-to-point index mapping, $n(u, v)$, and the pure map index, $f'(z)$. A similar procedure can be followed for the GMFE lens. Note that the refractive index of the circular MFE is calculated for $n_0 = 1$ in equation (1).

The proposed method is validated with a number of simulations using finite-elements based COMSOL multiphysics. The ray-tracing and electromagnetic modules are used for this purpose. The ray-tracing simulations were carried out for the MFE, mirrored MFE and GMFE with $m = 1/2$ and $m = 7/8$, see figures 1(a), (b), (d) and (f). Figure 4 illustrates the ray-tracing results when the conformal transformation is applied. We can conclude that the ray trajectories are transformed and adapted to the elliptical shape while maintaining the original functionality of the device.

The full wave simulations were carried out for an elliptical lens with a size of $20\lambda \times 15\lambda$. First, the functionality of the circular and elliptical mirrored MFE are examined for the TE (out-of-plane electrical field) and TM (out-of-plane magnetic field) polarizations excited with electric and magnetic line sources. Figures 5 and 6 illustrate the normalized field magnitudes. For figure 5, the excitation point is located at $(-3/4m, 0)$ whereas for figure 6, it is placed at $(0, 3/4m)$ for the circular MFE and $(0, 3/8m)$ for the elliptical one.

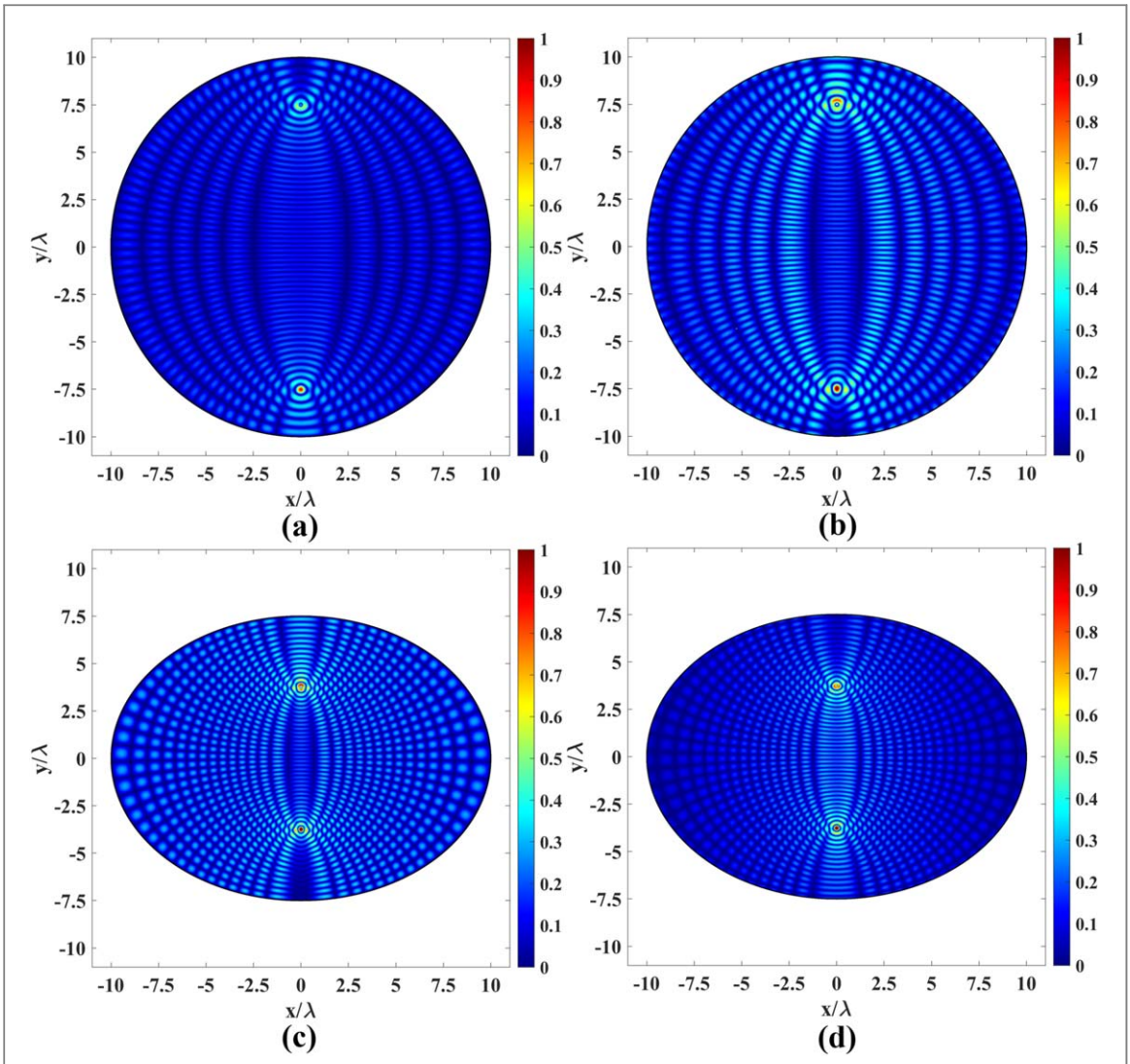

Figure 6. Normalized magnitude of the fields for the mirrored circular and elliptical MFE lenses for TE and TM polarizations. The excitation is applied at $(0, 3/4m)$ and $(0, 3/8m)$ for the circular MFE and elliptical MFE, respectively. (a) Magnitude of E_z and (b) magnitude of H_z for the circular MFE. (c) Magnitude of E_z and (d) magnitude of H_z for the elliptical MFE.

To provide a more accurate illustration of the results, a logarithmic representation of the field magnitude along $y = 0$ and $x = 0$ lines are drawn in figures 7 and 8. In these graphs, it is demonstrated that the imaging response is well preserved for both polarizations by the conformal transformation.

The previous simulations were conducted in a lossless dielectric medium that is derived from the conformal transformation. However, realizing a device with natural and synthesized dielectric materials will introduce an inherent loss tangent to the equations. The effect of the losses is an attenuation of the wave amplitude as it propagates inside the lens. This attenuation will be higher for a larger lens. We carried out the simulation of the previous MFE lens with losses, when excited at point $(-3/4m, 0)$ with an electric current line. The logarithmic magnitude of E_z is depicted along $y = 0$ for three cases in figure 9. The lossless case and the cases with $\tan\delta = 0.005$ and $\tan\delta = 0.01$ are compared. It is observed that the wave amplitude is affected by the loss but the functionality is preserved.

Figure 10 demonstrates the performance of the elliptical GMFE with parameter $m = 7/8$ (figure 1(f)) for splitting the power between two points. The excitation is applied for TE polarization at points $(-1m, 0)$ and $(0, 3/4m)$. The real and magnitude of E_z are depicted in figure 10. Scattering boundary conditions are used in this case to produce a better representation of the results.

The last simulation confirms the functionality of the elliptical GMFE with parameter $m = 1/2$ (figure 1(d)) as a monopole lens [129]. The excitation is applied for the TE polarization at points $(-1m, 0)$ and $(0, 3/4m)$. Figure 11 depicts the real part and magnitude of the E_z. Similar to the previous case, scattering boundary

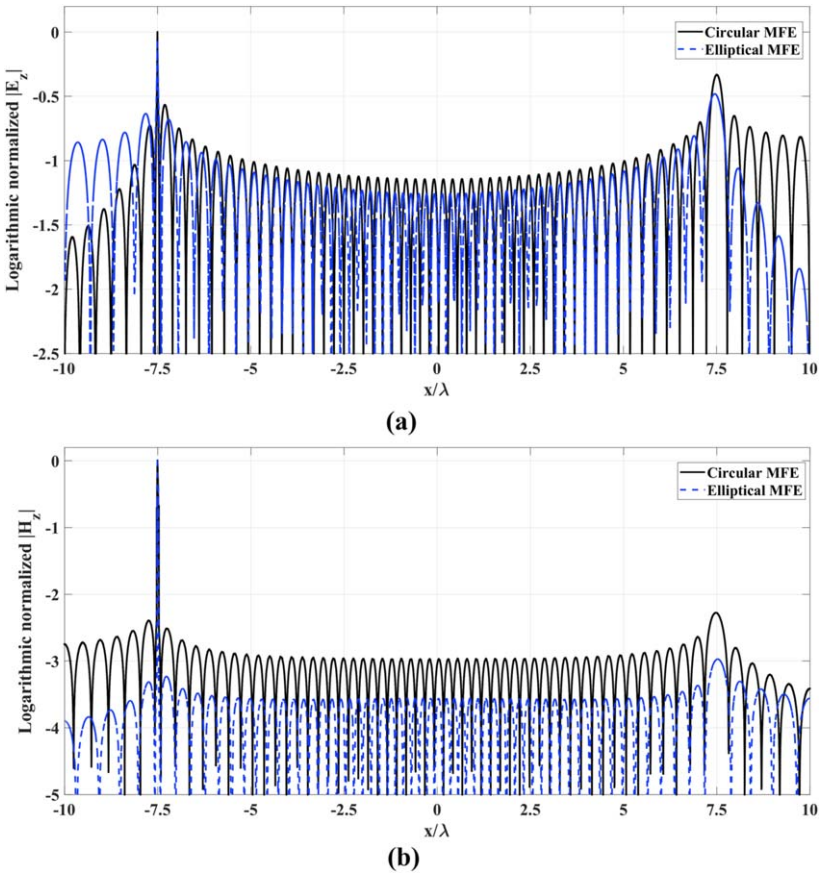

Figure 7. Logarithmic normalized magnitude of the fields along $y = 0$ line for the circular and elliptic MFE lenses. The excitation point is located at $(-3/4m, 0)$. (a) Magnitude of E_z and (b) magnitude of H_z.

conditions are used at the circumference. The wave refocuses on its source point after traversing the lens domain.

3. Conclusion

In this paper, we proposed and successfully implemented a closed-form formula for the conformal transformation between the interior of a circle and an ellipse. Compared to the available TO formulation for such mapping, our method provides a conformal approach that leads to an isotropic dielectric-only device. The unique closed-form formula can be employed to produce the desired compression ratio to circular lenses while keeping their optical properties unchanged owing to the essence of TO. Using this transformation, two GRIN lenses, the MFE and GMFE lenses were successfully compressed. The performance of GMFE lens is tested for a power splitting functionality and the case of the monopole lens. Both ray-tracing and full-wave simulations were carried out to verify the method.

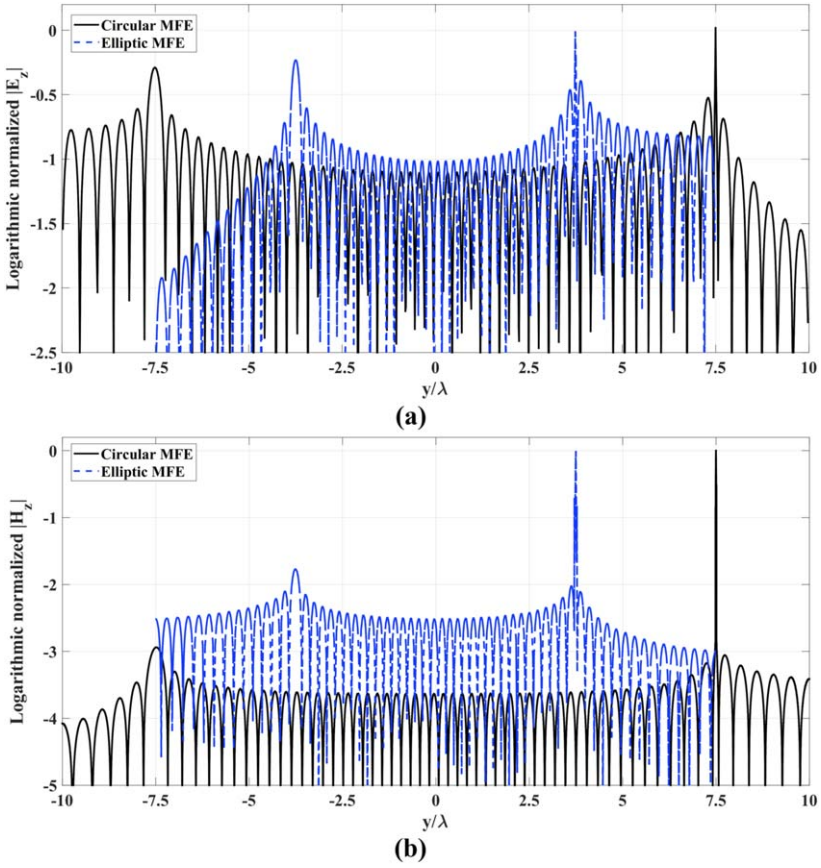

Figure 8. Logarithmic normalized magnitude of the fields along $x = 0$ line for the circular and elliptic MFE lenses. The excitation points are located at $(0, 3/4m)$ and $(0, 3/8m)$ for the circular and elliptical cases. (a) Magnitude of E_z and (b) magnitude of H_z.

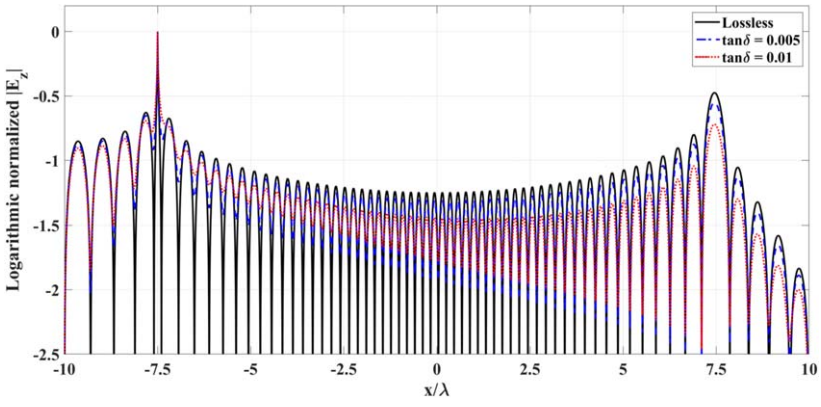

Figure 9. Logarithmic normalized magnitude of E_z along $y = 0$ line for the elliptic MFE lens with the excitation point located at $(-3/4m, 0)$ for the lossless case (solid black line), tan $\delta = 0.005$ (blue dashed line) and tan $\delta = 0.01$ (red dotted line).

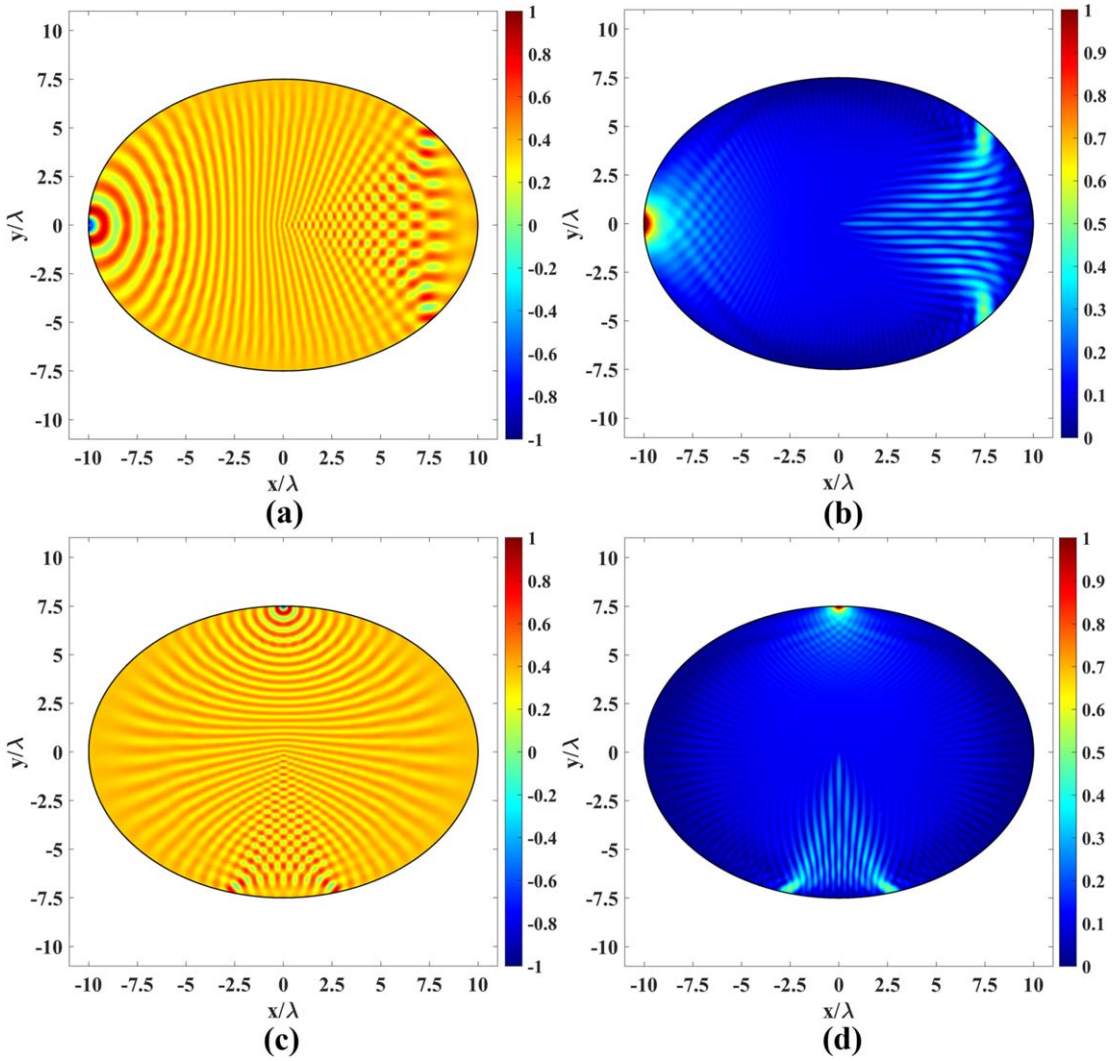

Figure 10. Normalized real part and magnitude of the electric fields for the elliptical GMFE with $m = 7/8$. (a) Real part and (b) magnitude of E_z, for an excitation at $(-1m, 0)$. (c) Real part and (d) magnitude of E_z, for an excitation at $(0, 3/4m)$.

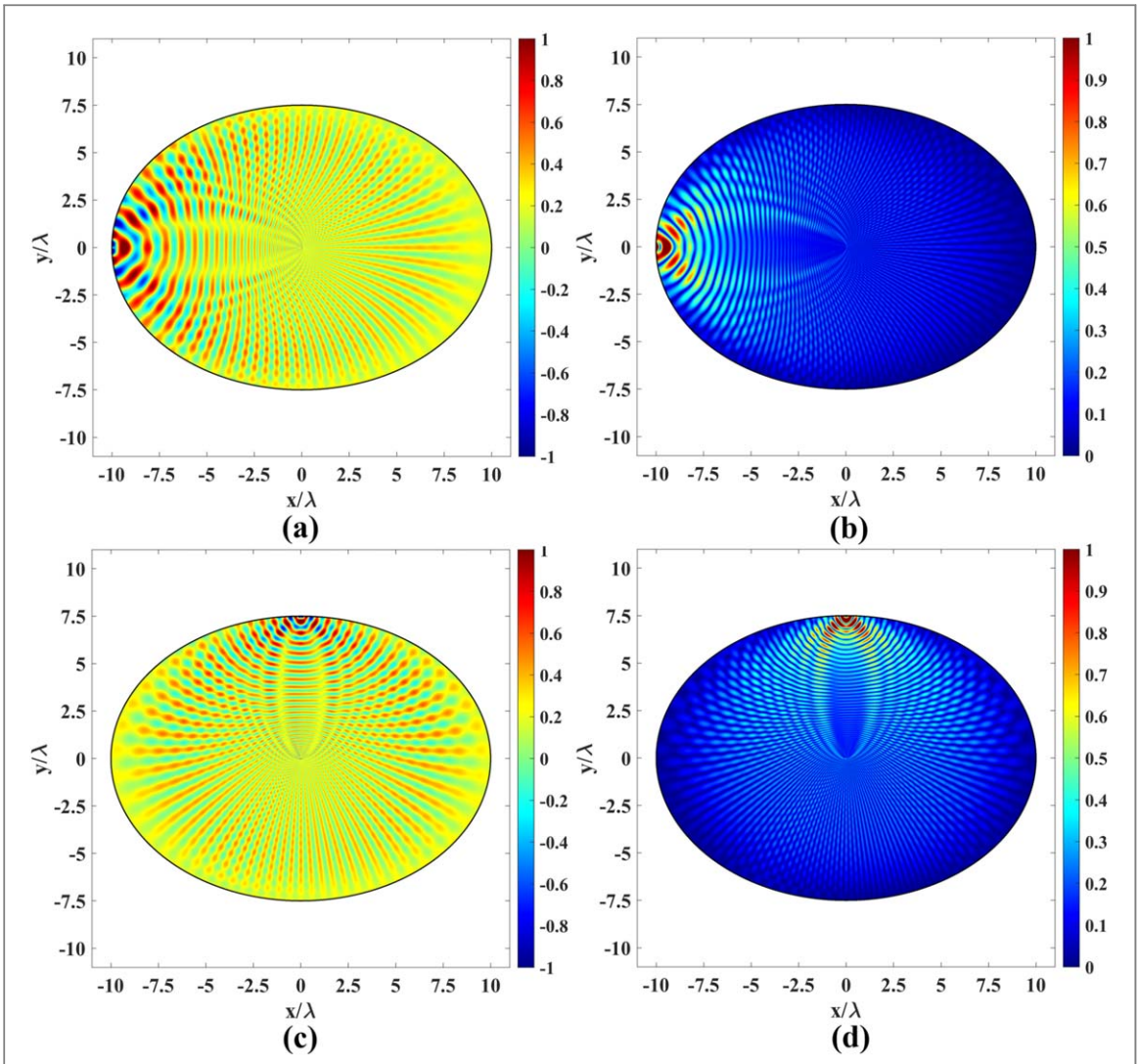

Figure 11. Normalized real part and magnitude of the electric fields for the elliptical GMFE with $m = 1/2$. (a) Real part and (b) magnitude of E_z, for an excitation at $(-1m, 0)$. (c) Real part and (d) magnitude of E_z, for an excitation at $(0, 3/4m)$.

Appendix A. TO in the case of conformal transformation

Once the mapping that transforms the physical elliptical space z to the virtual space in the unit disk w is derived, the refractive index can be calculated. The complex variables $z = x + iy$ and $w = u + iv$ indicate the coordinates of the space. The refractive index of the physical space is denoted by $n(x, y)$ and the one of virtual space by $n(u, v)$ as illustrated in figure A1. Here, for simplicity, we will assume that the medium in the virtual space is non-homogeneous and made of only dielectric materials ($\mu(u, v) = 1$) which is the case for GRIN lenses.

Based on the 2D TO formulation, the relative permittivity and permeability of these spaces are linked as follows [63]:

$$\varepsilon(u, v) = \frac{J\varepsilon(x, y)J^T}{\det(J)}, \tag{A.1}$$

$$1 = \frac{J\mu(x, y)J^T}{\det(J)}, \tag{A.2}$$

$$J = \begin{bmatrix} u_x & u_y & 0 \\ v_x & v_y & 0 \\ 0 & 0 & 1 \end{bmatrix} = \begin{bmatrix} u_x & u_y & 0 \\ -u_y & u_x & 0 \\ 0 & 0 & 1 \end{bmatrix}, \tag{A.3}$$

where J denotes the jacobian matrix of the transformation between the two spaces and the Cauchy–Riemann condition ($u_x = v_y, u_y = -v_x$) is applied to the Jacobian matrix. The final relative permittivity and permeability

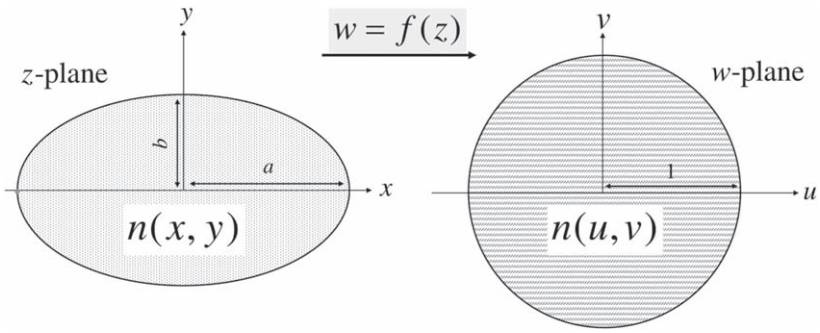

Figure A1. Schematic of the elliptical physical space and the corresponding circular virtual space.

of the physical space are calculated as follows:

$$\varepsilon(x,\,y) = \varepsilon(u,\,v)\begin{bmatrix} 1 & 0 & 0 \\ 0 & 1 & 0 \\ 0 & 0 & |f'(z)|^2 \end{bmatrix}, \tag{A.4}$$

$$\mu(x,\,y) = \begin{bmatrix} 1 & 0 & 0 \\ 0 & 1 & 0 \\ 0 & 0 & |f'(z)|^2 \end{bmatrix}, \tag{A.5}$$

with $|f'(z)|^2 = u_x^2 + u_y^2$.

The TE (E_z, H_x, H_y) mode is only affected by the μ_{xx}, μ_{xy}, μ_{yx}, μ_{yy} and ε_{zz} components of the medium, so the material of equation (A.4) and equation (A.5) can be simplified as:

$$\varepsilon(x,\,y) = \varepsilon(u,\,v)|f'(z)|^2, \tag{A.6}$$

$$\mu(x,\,y) = 1. \tag{A.7}$$

Hence, if the refractive index of the circular virtual space is known, the refractive index of the elliptical physical space can be calculated by the following equation:

$$n(x,\,y) = |f'(z)|\; n(u,\,v). \tag{A.8}$$

Appendix B. Schwarz–Christoffel transormation for calculation of a conformal maps from a rectangle to the upper half-plane and a rectangle to an ellipse

To derive the conformal map between an ellipse and a circle, two preliminary conformal maps must be elaborated. They are the conformal maps of a rectangle to the upper half-space and a rectangle to an ellipse. More details on functions and their features discussed in the current and next appendix can be found in conformal mapping handbooks [130–132]. If we could find the conformal map of a shape to some canonical domain like upper half-plane or a unit circle, we can map shapes to each other by two consecutive conformal transformations. Schwarz–Christoffel mapping was proposed to overcome the difficulty of finding such conformal map to a canonical domain. This mapping deals with the problem of mapping the upper half-plane to an arbitrary polygons. The general formulation for the mapping from the upper half-plane w with $w = u + iv$ coordinates to the polygon in the z-plane with $z = x + iy$ coordinates having N vertices is described as follows:

$$z(w) = A\int_0^w \prod_{k=1}^{N} (w - w_k)^{-(1-\alpha_k/\pi)}\mathrm{d}w + B. \tag{B.1}$$

where w_k are real points on the u axis and α_k are the interior angles of the polygon. Complex constants A and B can cause rotation and translation to the transformation.

Now, we focus on the problem of mapping when the polygon is a rectangle. Figure B1 depicts the mapping problem.

Here, we take 4 points on the real axis of the w-plane to be $w = \pm 1,\ \pm(1/k)(0 < k < 1)$. Using equation (B.1) and knowing that the interior angles of a rectangle are $\pi/2$, the equation of mapping is derived as follows:

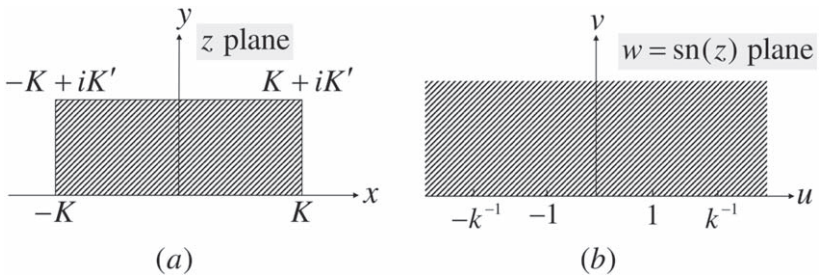

Figure B1. Schematic of the mapping, (a) Rectangle in the z-plane (b) Upper half-plane w.

Table B1. Vertices of the rectangular region in the z-plane and their corresponding points in the upper half-plane w-plane in figure B1.

z	K	$K + \mathrm{i}K'$	$\mathrm{i}K'$	$-K + \mathrm{i}K'$	$-K$	0
$w = \mathrm{sn}(z, k)$	1	k^{-1}	∞	$-k^{-1}$	-1	0

$$z(w) = \int_0^w \frac{\mathrm{d}w}{\sqrt{(1 - w^2)(1 - k^2w^2)}}, \tag{B.2}$$

which is known as the incomplete elliptical integral of the first kind. We label the vertices of rectangle as $\pm K$ and $\pm K + \mathrm{i}K'$. From equation (B.2), it is seen that the vertices of rectangle satisfy the following formulas:

$$\begin{aligned} K(k) &= \int_0^1 \frac{\mathrm{d}w}{\sqrt{(1 - w^2)(1 - k^2w^2)}}, \\ \mathrm{i}K'(k) &= \int_1^{k^{-1}} \frac{\mathrm{d}w}{\sqrt{(1 - w^2)(1 - k^2w^2)}}, \end{aligned} \tag{B.3}$$

where it can be shown that $K'(k) = K(\sqrt{1 - k^2})$. In the literature, K and K' are called complete and complementary complete elliptical integrals of the first kind which are apparently functions of paramter k. Note that parameter k makes the aspect ratio (AR) of the rectangle a free parameter. For a desired aspect ratio $\mathrm{AR} = K'(k)/K(k) = K(\sqrt{1 - k^2})/K(k)$, the corresponding k parameter is derived. The k parameter is also called the modulus for the elliptical integrals.

Here, we are interested in a function that is the inverse of equation (B.2) and maps the rectangle to the upper half-plane. This analytic function $w = \mathrm{sn}(z, k)$ is called 'The elliptic sine'. Table B1 shows the points involved in the mapping for both domains.

It is common to consider the parameter $q = \mathrm{e}^{-\frac{\pi K'(k)}{K(k)}}$ as the parameter that $\mathrm{sn}(z)$ depends on. Clearly, having the modulus k or parameter q are equivalent, and $w = \mathrm{sn}(z, q)$ is also a valid representation of the elliptic sine. As demonstrated later, in some problems, it is easier to calculate q based on the inputs. Modulus k can be expressed as an infinite series of q as follows:

$$k(q) = 4\sqrt{q} \prod_{n=1}^{\infty} \left(\frac{1 + q^{2n}}{1 + q^{2n-1}} \right)^4. \tag{B.4}$$

Also, k and the elliptic sine function must satisfy the following equations:

$$k(q) = \frac{2\sqrt{k(q^2)}}{1 + k(q^2)}, \tag{B.5}$$

$$\mathrm{sn}(z, q) = \frac{[1 + k(q^2)]\ \mathrm{sn}(\alpha z, q^2)}{1 + k(q^2)\ \mathrm{sn}^2(\alpha z, q^2)}, \ \alpha = [1 + k(q^2)]^{-1}. \tag{B.6}$$

Defining $\mathrm{sn}(K(q), q) = \mathrm{sn}(K(q^2), q^2) = 1$, the above equation results in $\mathrm{sn}(K(q^2), q^2) = \mathrm{sn}(K(q)/(1 + k(q^2)), q^2)$. Hence, we have the following identity:

$$K(q^2) = K(q)/(1 + k(q^2)). \tag{B.7}$$

Now, we investigate the function that maps the rectangle to the ellipse. Function $w = \sin(z)$ is known to have such property. Considering the rectangular $z = x + \mathrm{i}y$ region and taking $w = u + \mathrm{i}v$, we have:

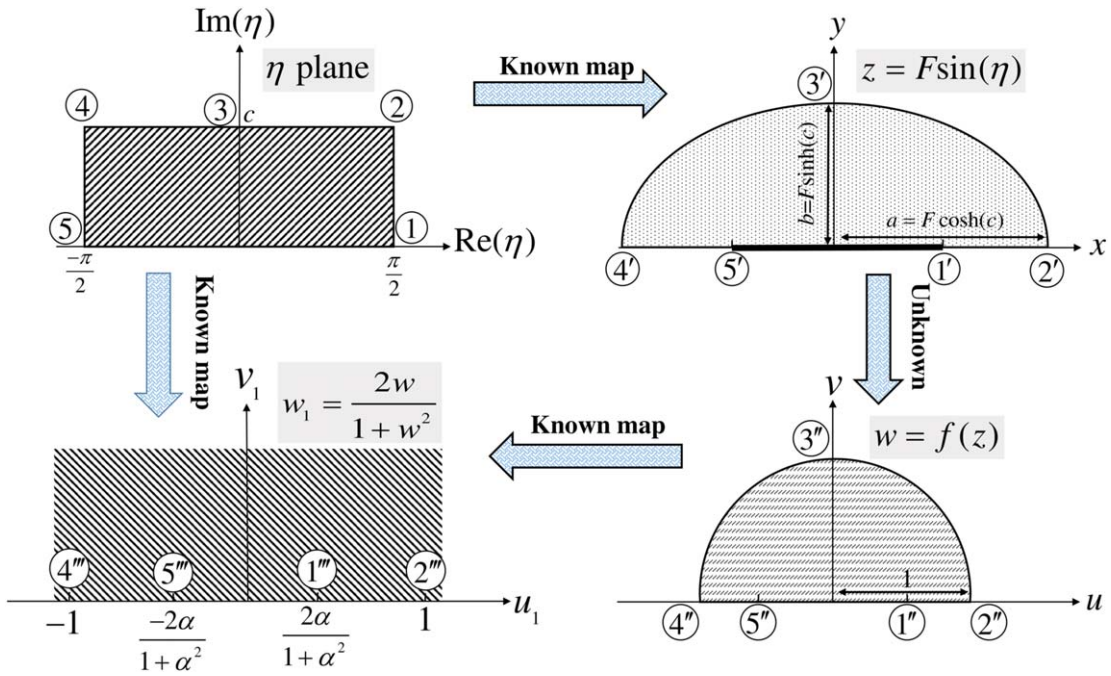

Figure C1. Schematic of the procedure to derive the conformal map from an ellipse to the unit circle.

Table C1. Mapping of points in the procedure of figure C1.

η	$\frac{\pi}{2}$	$\frac{\pi}{2}+ic$	ic	$\frac{-\pi}{2}+ic$	$\frac{-\pi}{2}$	0
$z=F\sin(\eta)$	F	a	bi	$-a$	$-F$	0
$w=f(z)$	α	1	i	-1	$-\alpha$	0
$w_1=\frac{2w}{1+w^2}$	$\frac{2\alpha}{1+\alpha^2}$	1	∞	-1	$\frac{-2\alpha}{1+\alpha^2}$	0

$$u+iv=\sin(z)=\sin(x+iy),$$
$$u=\sin(x)\cosh(y),\ v=i\cos(x)\sinh(y). \tag{B.8}$$

Hence, the following equations can be derived based on two well-known identities of $\sin^2(x)+\cos^2(x)=1$ and $\cosh^2(y)-\sinh^2(y)=1$:

$$\frac{u^2}{\cosh^2(y)}+\frac{v^2}{\sinh^2(y)}=1,$$
$$\frac{u^2}{\sin^2(x)}-\frac{v^2}{\cos^2(x)}=1, \tag{B.9}$$

which means $y=c$ lines get mapped to concentric ellipses with foci at ±1 and major and minor axes of $\cosh(c)$ and $\sinh(c)$ while $x=c$ lines are transformed to hyperbolas of half axes $\sin(c)$ and $\cos(c)$ with foci located again at ±1.

Appendix C. Conformal transformation of an ellipse to the unit disk $|w|\leqslant 1$

The conformal mapping of an ellipse to the unit circle is not straightforward and includes a combination of conformal maps. Here, function $w=f(z)$ carries out the mapping between the ellipse and the unit circle. If we suppose, $f(0)=0, f'(0)>0$ then, according to the symmetry principle, this mapping also maps the upper half of an ellipse to the upper half of the unit circle.

We start from a rectangular region of $\frac{-\pi}{2}<\mathrm{Re}\{\eta\}<\frac{\pi}{2}$, $0<\mathrm{Im}\{\eta\}<c$ and as it was mentioned in appendix B, it is understood that function $z=F\sin(\eta)$ maps horizontal lines in the η-plane to concentric ellipses

with foci located at $\pm F$ in the z-plane. The major and minor axes of the outer ellipse are $a = F\cosh(c)$ and $b = F\sinh(c)$, respectively. The whole procedure of finding the map is illustrated in figure C1. The original and the transformed points are labeled by the same number between the shapes.

The target function is $w = f(z) = f(F\sin(\eta))$ that performs our desired map. The upper half of the unit circle $|w| < 1$ is mapped to the upper half-plane by mapping $w_1 = 2w/(1 + w^2)$. As a result, the aforementioned rectangular region is mapped to the upper half-plane by the following mapping:

$$w_1 = \frac{2f(F\sin(\eta))}{1 + f^2(F\sin(\eta))}. \tag{C.1}$$

If we suppose that $f(F) = \alpha$, the mapping between points on each step of the mapping procedure can be summarized in table C1. Note that the points are arranged in columns based on their numbering in figure C1.

The first and last rows of table C1 show the corresponding points for mapping between a rectangle and the upper half-space. The formula for w_1 is obtained by comparing the results of the above table to the ones obtained from figure B1 and table B1:

$$w_1 = \frac{2f(F\sin(\eta))}{1 + f^2(F\sin(\eta))} = \frac{2\alpha}{1 + \alpha^2}\,\mathrm{sn}\left(\frac{2K(k)}{\pi}\eta,\, k\right), \tag{C.2}$$

where the $\frac{K'(k(q))}{K(k(q))} = \frac{2c}{\pi}$ holds for the aspect ratio and hence $q = e^{-2c} = \frac{a-b}{a+b}$. Also, the modulus for calculation of K, K' and sn function is $k(q)$ and satisfies the following equation:

$$k(e^{-2c}) = \frac{2\alpha}{1 + \alpha^2}. \tag{C.3}$$

The right hand side of equation (C.2) can be rewritten based on identities of equation (B.5) and equation (B.6):

$$\frac{2\alpha}{1 + \alpha^2}\,\mathrm{sn}\left(\frac{2K(q)}{\pi}\eta,\, q\right) = k(q)\,\mathrm{sn}\left(\frac{2K(q)}{\pi}\eta,\, q\right) = \frac{2\sqrt{k(q^2)}\,\mathrm{sn}(\beta\eta,\, q^2)}{1 + k(q^2)\,\mathrm{sn}^2(\beta\eta,\, q^2)}, \tag{C.4}$$

where $\beta = 2K(q)/\pi(1 + k(q^2))$. Based on equation (B.7), $\beta = 2K(q^2)/\pi$.

As a result, the equation for $w = f(z) = f(F\sin(\eta))$ function is obtained using equation (C.2) and equation (C.4):

$$f(F\sin(\eta)) = \sqrt{k(q^2)}\,\mathrm{sn}\left(\frac{2K(q^2)}{\pi}\eta,\, q^2\right). \tag{C.5}$$

Hence, the interior of the ellipse $x^2/a^2 + y^2/b^2 = 1$ with foci located at $F = \pm\sqrt{a^2 - b^2}$ in the z-plane gets mapped to the interior of the unit circle $|w| \leqslant 1$ in the w-plane by the following conformal map:

$$w = f(z) = \sqrt{k(q^2)}\,\mathrm{sn}\left(\frac{2K(q^2)}{\pi}\sin^{-1}\left(\frac{z}{F}\right),\, q^2\right),\quad q^2 = e^{-4c} = \left(\frac{a-b}{a+b}\right)^2. \tag{C.6}$$

Having the axes lengths of the ellipse, the q parameter can be calculated. The modulus for this particular q is derived using equation (B.4) and, then, the mapping can also be calculated. Note that since for our application we require points a, bi, $-a$ and $-b$i on the ellipse circumference to be mapped respectively to 1, i, -1 and $-$i on the unity circle boundary, based on the Riemann mapping theorem, this mapping is unique regardless of the approach followed to derive the transformation formula [133].

Based on equation (A.8), the refractive index formula for such transformation is as follows:

$$n(x,\, y) = \left| \frac{2K(q^2)\sqrt{k(q^2)}}{\pi\sqrt{F^2 - z^2}}\,\mathrm{cn}\left(\frac{2K(q^2)}{\pi}\sin^{-1}\left(\frac{z}{F}\right),\, q^2\right) \times \mathrm{dn}\left(\frac{2K(q^2)}{\pi}\sin^{-1}\left(\frac{z}{F}\right),\, q^2\right)\right| n(u,\, v), \tag{C.7}$$

where cn and dn function are called 'elliptic cosine' and 'delta amplitude' functions, respectively. $n(u, v)$ is the coordinate transformed refractive index that depends on whether one chooses to transform the MFE or GMFE. It can be calculated by replacing 'r' in equation (1) or equation (2) by $|w|$ of equation (C.6).

In addition, the inverse of the equation (C.6) map is calculated as below:

$$z = f^{-1}(w) = F\sin\left(\frac{\pi}{2K(q^2)}\int_0^{\frac{w}{\sqrt{k(q^2)}}}\frac{\mathrm{d}t}{\sqrt{(1 - t^2)(1 - k^2(q^2)t^2)}}\right), \tag{C.8}$$

where the integral term is the inverse elliptical sine function $\mathrm{sn}^{-1}(w/\sqrt{k(q^2)}, k(q^2))$. Equation (C.8) can be solved either by numerical integration or using 'InverseJacobiSN' function in Mathematica that employs hypergeometric functions to calculate the integral value [134].

ORCID iDs

Hossein Eskandari https://orcid.org/0000-0003-2846-3368
Mohammad Saeed Majedi https://orcid.org/0000-0001-5846-5773

References

[1] Liu R, Cheng Q, Chin J Y, Mock J J, Cui T J and Smith D R 2009 *Opt. Express* **17** 21030–41
[2] Pfeiffer C and Grbic A 2010 *IEEE Trans. Antennas Propag.* **58** 3055–9
[3] Quevedo-Teruel O, Miao J, Mattsson M, Algaba-Brazalez A, Johansson M and Manholm L 2018 *IEEE Antennas Wirel. Propag. Lett.* **17** 1588–92
[4] Ma H F and Cui T J 2010 *Nat. Commun.* **1** 124
[5] Quevedo-Teruel O, Tang W, Mitchell-Thomas R C, Dyke A, Dyke H, Zhang L, Haq S and Hao Y 2013 *Sci. Rep.* **3** 1903
[6] Ma H F and Cui T J 2010 *Nat. Commun.* **1** 21
[7] Taskhiri M M and Amirhosseini M K 2017 *J. Opt. Soc. Am.* A **34** 1265–71
[8] Koike Y, Sumi Y and Ohtsuka Y 1986 *Appl. Opt.* **25** 3356–63
[9] Koike Y, Kanemitsu A, Shioda Y, Nihei E and Ohtsuka Y 1994 *Appl. Opt.* **33** 3394–400
[10] Gunderson L C and Holmes G T 1968 *Appl. Opt.* **7** 801–4
[11] Peeler G and Coleman H 1958 *IRE Trans. Anntenas Propag.* **6** 202–7
[12] Fuchs B, Lafond O, Rondineau S and Himdi M 2006 *IEEE Trans. Microwave Theory Tech.* **54** 2292–300
[13] Lv H, Shi B, Guo L and Liu A 2008 *J. Opt. Soc. Am.* A **25** 609–11
[14] Liu J, Mendis R and Mittleman D M 2013 *Appl. Phys. Lett.* **103** 031104
[15] Mitchell-Thomas R C, Quevedo-Teruel O, Sambles J R and Hibbins A P 2016 *Sci. Rep.* **6** 30984
[16] Mendis R, Liu J and Mittleman D M 2012 *Appl. Phys. Lett.* **101** 111108
[17] Gabrielli L H and Lipson M 2011 *Opt. Express* **19** 20122–7
[18] Falco A D, Kehr S C and Leonhardt U 2011 *Opt. Express* **19** 5156–62
[19] Aghanejad I, Abiri H and Yahaghi A 2012 *IEEE Trans. Antennas Propag.* **60** 4074–81
[20] Gaufillet F and Akmansoy E 2018 *IEEE Photonics J.* **10** 1–10
[21] Gilarlue M, Badri S H, Saghai H R, Nourinia J and Ghobadi C 2018 *Photonics Nanostruct. Fundam. Appl.* **31** 154–9
[22] Gilarlue M, Nourinia J, Ghobadi C, Badri S H and Saghai H R 2019 *Opt. Commun.* **435** 385–93
[23] Zentgraf T, Valentine J, Tapia N, Li J and Zhang X 2010 *Adv. Mater.* **22** 2561–4
[24] Gabrielli L H and Lipson M 2010 *J. Opt.* **13** 024010
[25] Zentgraf T, Liu Y, Mikkelsen M H, Valentine J and Zhang X 2011 *Nat. Nanotechnol.* **6** 151–5
[26] Bitton O, Bruch R and Leonhardt U 2018 *Phys. Rev. Appl.* **10** 044059
[27] Dockrey J A, Lockyear M J, Berry S J, Horsley S A R, Sambles J R and Hibbins A P 2013 *Phys. Rev.* B **87** 125137
[28] Maci S, Minatti G, Casaletti M and Bosiljevac M 2011 *IEEE Antennas Wirel. Propag. Lett.* **10** 1499–502
[29] Prado D R, Osipov A V and Quevedo-Teruel O 2015 *Opt. Lett.* **40** 926–9
[30] Quevedo-Teruel O, Ebrahimpouri M and Kehn M N M 2016 *IEEE Antennas Wirel. Propag. Lett.* **15** 484–7
[31] Bosiljevac M, Casaletti M, Caminita F, Sipus Z and Maci S 2012 *IEEE Trans. Antennas Propag.* **60** 4065–73
[32] Maxwell J C 1854 *Cambridge Dublin Math. J.* **8** 188–95
[33] Demkov Y N and Ostrovsky V N 1971 *Sov. Phys. JETP* **33** 1083–7
[34] Ma Y G, Ong C K, Tyc T and Leonhardt U 2009 *Nat. Mater.* **8** 639–42
[35] Tyc T, Herzánová L, vSarbort M and Bering K 2011 *New J. Phys.* **13** 115004
[36] Miñano J C 2006 *Opt. Express* **14** 9627–35
[37] Perczel J, Tyc T and Leonhardt U 2011 *New J. Phys.* **13** 083007
[38] Luneberg R 1964 *Mathematical Theory of Optics* (Berkeley, CA: University of California Press)
[39] Guenneau S, Diatta A and McPhedran R 2010 *J. Mod. Opt.* **57** 511–27
[40] Leonhardt U 2009 *New J. Phys.* **11** 093040
[41] Leonhardt U and Philbin T G 2010 *Phys. Rev.* A **81** 011804
[42] Leonhardt U and Sahebdivan S 2011 *J. Opt.* **13** 024016
[43] Leonhardt U 2010 *New J. Phys.* **12** 058002
[44] Leonhardt U and Philbin T G 2010 *Phys. Rev.* A **82** 057802
[45] Leonhardt U 2011 *New J. Phys.* **13** 028002
[46] Tyc T and Zhang X 2011 *Nature* **480** 42–3
[47] Miñano J C, Marqués R, González J C, Benítez P, Delgado V, Grabovickic D and Freire M 2011 *New J. Phys.* **13** 125009
[48] Miñano J C, Sánchez-Dehesa J, González J C, Benítez P, Grabovičkić D, Carbonell J and Ahmadpanahi H 2014 *New J. Phys.* **16** 033015
[49] Blaikie R J 2010 *New J. Phys.* **12** 058001
[50] Merlin R 2010 *Phys. Rev.* A **82** 057801
[51] Merlin R 2011 *J. Opt.* **13** 024017
[52] Blaikie R J 2011 *New J. Phys.* **13** 125006
[53] Kinsler P and Favaro A 2011 *New J. Phys.* **13** 028001
[54] Tyc T and Danner A 2014 *New J. Phys.* **16** 063001
[55] Xu H and Shi Y 2018 *Laser Photonics Rev.* **12** 1800094
[56] Fuchs B, Lafond O, Rondineau S, Himdi M and Coq L L 2007 *IEEE Trans. Antennas Propag.* **55** 479–82
[57] Fuchs B, Lafond O, Palud S, Coq L L, Himdi M, Buck M C and Rondineau S 2008 *IEEE Trans. Antennas Propag.* **56** 3058–62
[58] Mei Z L, Bai J, Niu T M and Cui T J 2012 *IEEE Trans. Antennas Propag.* **60** 398–401

[59] Huang M, Yang S, Gao F, Quarfoth R and Sievenpiper D 2014 *IEEE Antennas Wirel. Propag. Lett.* **13** 365–8
[60] Xu H X, Wang G M, Tao Z and Cai T 2014 *IEEE Trans. Antennas Propag.* **62** 4823–8
[61] Shi Y, Li K, Wang J, Li L and Liang C H 2015 *IEEE Trans. Antennas Propag.* **63** 3742–7
[62] Lei Q, Foster R, Grant P S and Grovenor C 2017 *IEEE Trans. Microwave Theory Tech.* **65** 4823–35
[63] Pendry J B 2006 *Science* **312** 1780–2
[64] Leonhardt U 2006 *Science* **312** 1777–80
[65] Leonhardt U and Philbin T G 2006 *New J. Phys.* **8** 247
[66] Schurig D, Mock J J, Justice B J, Cummer S A, Pendry J B, Starr A F and Smith D R 2006 *Science* **314** 977–80
[67] Cai W, Chettiar U K, Kildishev A V, Shalaev V M and Milton G W 2007 *Appl. Phys. Lett.* **91** 111105
[68] Cai W, Chettiar U K, Kildishev A V and Shalaev V M 2007 *Nat. Photonics* **1** 224–7
[69] Yan W, Yan M, Ruan Z and Qiu M 2008 *New J. Phys.* **10** 043040
[70] Yan W, Yan M and Qiu M 2008 *Appl. Phys. Lett.* **93** 021909
[71] Li J and Pendry J B 2008 *Phys. Rev. Lett.* **101** 203901
[72] Liu R, Ji C, Mock J J, Chin J Y, Cui T J and Smith D R 2009 *Science* **323** 366–9
[73] Kwon D H and Werner D H 2008 *Opt. Express* **16** 18731–8
[74] Mousavi S S S, Majedi M S and Eskandari H 2017 *Optik* **130** 1099–106
[75] Eskandari H, Majedi M S and Attari A R 2017 *Optik* **135** 407–16
[76] Eskandari H, Majedi M S and Attari A R 2017 *J. Opt. Soc. Am.* B **34** 1191–8
[77] Teixeira P A, Silva D G, Gabrielli L H, Spadoti D H and Junqueira M A F C 2018 *Opt. Eng.* **57** 037111
[78] Eskandari H, Attari A R and Majedi M S 2018 *J. Opt. Soc. Am.* B **35** 1585–95
[79] Ma H, Qu S, Xu Z and Wang J 2008 *Opt. Express* **16** 22072–82
[80] Lin L, Wang W, Cui J, Du C and Luo X 2008 *Opt. Express* **16** 6815–21
[81] Shu W, Yang S, Yan W, Ke Y and Smith T 2015 *Opt. Commun.* **338** 307–12
[82] Kwon D H and Werner D H 2008 *New J. Phys.* **10** 115023
[83] Kwon D H and Werner D H 2009 *Opt. Express* **17** 7807–17
[84] Kundtz N and Smith D R 2009 *Nat. Mater.* **9** 129–32
[85] Roberts D A, Kundtz N and Smith D R 2009 *Opt. Express* **17** 16535–42
[86] Tang W, Argyropoulos C, Kallos E, Song W and Hao Y 2010 *IEEE Trans. Antennas Propag.* **58** 3795–804
[87] Wu Q, Jiang Z H, Quevedo-Teruel O, Turpin J P, Tang W, Hao Y and Werner D H 2013 *IEEE Trans. Antennas Propag.* **61** 5910–22
[88] Mateo-Segura C, Dyke A, Dyke H, Haq S and Hao Y 2014 *IEEE Trans. Antennas Propag.* **62** 1945–53
[89] Jain S, Mittra R and Pandey S 2015 *J. Electromagn. Waves Appl.* **29** 1329–41
[90] Ebrahimpouri M and Quevedo-Teruel O 2017 *IEEE Trans. Antennas Propag.* **65** 2256–64
[91] Su Y and Chen Z N 2018 *IEEE Trans. Antennas Propag.* **66** 5088–97
[92] Chen H and Chan C T 2007 *Appl. Phys. Lett.* **90** 241105
[93] Chen H, Hou B, Chen S, Ao X, Wen W and Chan C T 2009 *Phys. Rev. Lett.* **102** 183903
[94] Rahm M, Schurig D, Roberts D A, Cummer S A, Smith D R and Pendry J B 2008 *Photonics Nanostruct. Fundam. Appl.* **6** 87–95
[95] Bian B, Liu S, Wang S, Kong X, Guo Y, Zhao X, Ma B and Chen C 2013 *Opt. Express* **21** A231–40
[96] Wang S Y, Yu B, Liu S and Bian B 2013 *J. Opt. Soc. Am.* A **30** 1563–7
[97] Rahm M, Roberts D A, Pendry J B and Smith D R 2008 *Opt. Express* **16** 11555–67
[98] Gabrielli L H, Liu D, Johnson S G and Lipson M 2012 *Nat. Commun.* **3** 1217
[99] Viaene S, Ginis V, Danckaert J and Tassin P 2016 *Phys. Rev.* B **93** 085429
[100] Emiroglu C D and Kwon D H 2010 *J. Appl. Phys.* **107** 084502
[101] García-Meca C, Tung M M, Galán J V, Ortuño R, Rodríguez-Fortuño F J, Martí J and Martínez A 2011 *Opt. Express* **19** 3562–75
[102] Xu H Y, Zhang B, Barbastathis G and Sun H D 2011 *J. Opt. Soc. Am.* B **28** 2633–6
[103] Markov P, Valentine J G and Weiss S M 2012 *Opt. Express* **20** 14705–13
[104] Cao J, Zhang L, Yan S and Sun X 2014 *Appl. Phys. Lett.* **104** 191102
[105] Eskandari H, Majedi M S and Attari A R 2017 *Appl. Opt.* **56** 5599–606
[106] Eskandari H, Attari A R and Majedi M S 2017 *J. Opt. Soc. Am.* B **35** 54–60
[107] Eskandari H, Quevedo-Teruel O, Attari A R and Majedi M S 2019 *Opt. Mater. Express* **9** 1320–32
[108] Landy N I and Padilla W J 2009 *Opt. Express* **17** 14872–9
[109] Xu L and Chen H 2014 *Nat. Photonics* **9** 15–23
[110] Chang Z, Zhou X, Hu J and Hu G 2010 *Opt. Express* **18** 6089–96
[111] Schmiele M, Varma V S, Rockstuhl C and Lederer F 2010 *Phys. Rev.* A **81** 033837
[112] Yao K and Jiang X 2011 *J. Opt. Soc. Am.* B **28** 1037–42
[113] Mei Z L, Bai J and Cui T J 2011 *New J. Phys.* **13** 063028
[114] Wu Q, Turpin J P and Werner D H 2012 *Light: Science & Applications* **1** e38
[115] Yi J, Burokur S N, Piau G P and de Lustrac A 2016 *J. Opt.* **18** 044010
[116] Yang R, Tang W and Hao Y 2011 *IEEE Antennas Wirel. Propag. Lett.* **10** 1290–4
[117] Liang L and Hum S V 2013 *Opt. Express* **21** 2133–46
[118] Liang L and Hum S V 2014 *IEEE Trans. Antennas Propag.* **62** 2481–7
[119] Smith D R, Urzhumov Y, Kundtz N B and Landy N I 2010 *Opt. Express* **18** 21238–51
[120] Hunt J, Jang G and Smith D R 2011 *J. Opt. Soc. Am.* B **28** 2025–9
[121] Yang F, Mei Z L and Cui T J 2014 *Appl. Phys. Lett.* **104** 073510
[122] Li S, Zhou Y, Dong J, Zhang X, Cassan E, Hou J, Yang C, Chen S, Gao D and Chen H 2018 *Optica* **5** 1549–56
[123] Tao S, Zhou Y and Chen H 2019 *Phys. Rev.* A **99** 013837
[124] Mikaelian A and Prokhorov A 1980 Self-focusing media with variable index of refraction progress in optics *Progress in Optics* vol 17 (Amsterdam: Elsevier) ch 5 pp 279–345
[125] Tyc T, Dao H L and Danner A J 2015 *Phys. Rev.* A **92** 053827
[126] Wang X, Chen H, Liu H, Xu L, Sheng C and Zhu S 2017 *Phys. Rev. Lett.* **119** 033902
[127] Demetriadou A and Hao Y 2011 *Opt. Express* **19** 19925–34
[128] Demetriadou A and Hao Y 2011 *IEEE Antennas Wirel. Propag. Lett.* **10** 1590–3
[129] Horsley S A R, Hooper I R, Mitchell-Thomas R C and Quevedo-Teruel O 2014 *Sci. Rep.* **4** 4876
[130] Nehari Z 1952 *Conformal Mapping, International Series in Pure and Applied Mathematics* (New York: McGraw-Hill)

[131] Abramowitz M and Stegun I A (ed) 1965 *Handbook of Mathematical Functions: With Formulas, Graphs, and Mathematical Tables, Dover Books on Mathematics* (New York: Dover)
[132] Driscoll T A and Trefethen L N 2009 *Schwarz-Christoffel Mapping, Cambridge Monographs on Applied and Computational Mathematics* (Cambridge: Cambridge University Press)
[133] Lawler G F 2005 *Conformally Invariant Processes in the Plane* (Providence, RI: American Mathematical Society)
[134] Cvijovic D and Klinowski J 1994 *Proc. R. Soc.* A **444** 525–32